Published in final edited form as:

Nat Struct Mol Biol. 2014 September ; 21(9): 794–802. doi:10.1038/nsmb.2867.

RNA polymerase pausing and nascent RNA structure formation are linked through clamp domain movement

Pyae P. Hein[1], **Kellie E. Kolb**[1], **Tricia Windgassen**[1], **Michael J. Bellecourt**[1], **Seth A. Darst**[2], **Rachel A. Mooney**[1], and **Robert Landick**[1,3,4]

[1]Department of Biochemistry, University of Wisconsin – Madison, Madison, WI 53706, USA

[2]Laboratory of Molecular Biophysics, The Rockefeller University, New York, NY 10065, USA

[3]Department of Bacteriology, University of Wisconsin – Madison, Madison, WI 53706, USA

Abstract

The rates of RNA synthesis and nascent RNA folding into biologically active structures are linked via pausing by RNA polymerase (RNAP). Structures that form within the RNA exit channel can increase pausing by interacting with bacterial RNAP or decrease pausing by preventing backtracking. Conversely, pausing is required for proper folding of some RNAs. Opening of the RNAP clamp domain is proposed to mediate some effects of nascent RNA structures. However, the connections among RNA structure formation, clamp movement, and catalytic activity remain uncertain. We assayed exit-channel structure formation in *Escherichia coli* RNAP together with disulfide crosslinks that favor closed or open clamp conformations and found that clamp position directly influences RNA structure formation and catalytic activity. We report that exit-channel RNA structures slow pause escape by favoring clamp opening and through interactions with the flap that slow translocation.

INTRODUCTION

Although it has been appreciated for decades that folding of RNA into biologically active structures is controlled by the rate of RNA synthesis by RNA polymerase (RNAP)[1,2], the mechanisms by which RNAP guides RNA folding remain poorly understood. Pausing by both bacterial RNAP and eukaryotic RNAPII can guide proper RNA folding[3–10]. Conversely, RNA structures can influence the rate of transcript elongation either by prolonging pausing through interactions in the RNA exit channel[11] or by sterically blocking reverse translocation (backtracking) of the RNA 3′ end out of the RNAP active site[12,13].

[4]To whom correspondence should be addressed. Fax: 608-262-9865; landick@biochem.wisc.edu.

AUTHOR CONTRIBUTIONS

P.P.H, R.L., S.A.D., and R.A.M. designed the experiments. P.P.H., K.E.K., T.W., M.J.B., and R.A.M. performed the experiments and data analysis. P.P.H. and R.L. wrote the manuscript.

COMPETING FINANCIAL INTERESTS

The authors declare no competing financial interests.

The interplay of RNA folding and transcriptional pausing and their modulation by RNAP and associated regulators has been studied most extensively in bacteria. In *E. coli*, transient pauses that occur about ten times per kb on average[14,15] are thought to arise by a sequence-induced rearrangement of the RNAP active site that blocks loading of the template base[16]. This "elemental" pause allows time for RNA structure formation, for backtracking, or for regulator or ribosome interactions[16–18]. The elemental paused elongation complexes (ePECs) thus serve as regulatory intermediates whose duration can be modified by nascent RNA structures known to form within the RNA exit channel of RNAP. A duplex stem that extends to −13 or −12 (exit-channel duplex; Fig. 1a) increases pause dwell times by factors of 10 or more[11,19] through interactions with RNAP. These interactions are thought to require the flap tip on one side of the RNA exit channel[20] and to affect the RNA active site by stabilizing an open conformation of the clamp domain on the other side of the exit channel (Fig. 1a,b)[16,21,22]. NusA enhances pause-stimulation by exit-channel duplexes ≥8 bp[23] *via* contacts of its N-terminal domain (NTD) with the duplex and the flap tip[24], and promotes formation of biologically active ribozymes and riboswitches[6,7,9]. In contrast, the NusG NTD (or the paralogous RfaH NTD) suppresses effects of exit-channel duplexes through contacts that appear to stabilize a closed-clamp conformation and to compete with duplex formation[23,25]. However, whether RNAP actively modulates RNA structure formation through exit-channel contacts (in addition to controlling the rate of RNA synthesis) is unknown and the mechanism by which exit-channel duplexes increase pausing is incompletely understood.

The hairpin-stimulated pause in the *E. coli his* operon leader region provides a useful model to investigate these issues. Here, a 5-bp stem, 8-nt loop "pause hairpin" forms 12 nt from the RNA 3′ end after RNAP enters the elemental pause state, prolongs pausing to synchronize transcription and translation during attenuation, and can be mimicked by an 8-bp duplex formed with an antisense RNA (asRNA)[23,24]. The pause hairpin or duplex inhibits translocation and also prevents formation of a helical hairpin form of the trigger loop (TL) required for rapid catalysis in the RNAP active site[21,22]. An open-clamp conformation of RNAP stabilized by the pause hairpin is postulated to inhibit TL folding into the trigger helices (TH) *via* interactions with the bridge helix (BH)[21]. However, the energetic connections among hairpin formation, clamp movement, TL-folding, and inhibited translocation are unknown.

To investigate these connections, we implemented two new probes of RNAP structure and activity. First, we developed a way to measure RNA duplex formation in the RNAP exit channel using asRNA binding to and quenching of fluorophore-containing nascent RNA. The use of asRNA allows measurement of duplex formation energetics in ways not possible for the natural hairpin. Second, we engineered disulfide crosslinks that favor the closed or open conformations of RNAP. By manipulating clamp position, we could deconvolute effects of the clamp from effects of the exit-channel duplex. Using these assays together with RNAP alterations known to affect the exit channel or active site, elongation regulators RfaH and NusA, and established assays of pausing[11,23,26] and translocation[27,28], we determined the effects of RNAP and clamp position on RNA structure formation and the energetic linkage of the exit channel and active site through clamp conformation.

RESULTS

The RNAP exit channel permits formation of RNA structures

To assay how the RNAP exit channel affects formation of nascent RNA structures, we used fluorescence quenching of pyrrolo-cytosine (PC; 3-[β-D-2-ribofuranosyl]-6-methylpyrrolo [2,3-d]pyrimidin-2(3H)-one)[29,30] positioned near the 5′ end of the nascent RNA in an ePEC scaffold (Fig. 1a). PC forms Watson-Crick base pairs with G similarly to unmodified C and is quenched by stacking interactions with adjacent bases in duplex structures[29–32]. To reduce stacking in the ssRNA and increase fluorescence of unpaired PC, we located PC between pyrimidines (5′-U-PC-C-3′). Duplex formation by the PC RNA alone and an 8-nt antisense RNA (asRNA) was readily detectable by an ~15% decrease in PC fluorescence; a noncomplementary 8-nt RNA gave insignificant change in PC fluorescence (Supplementary Figs. 1a–d). These results are consistent with previous measurements of PC fluorescence quenching in DNA[33] or RNA[34].

RNAP could inhibit formation of exit-channel duplexes sterically (Fig. 1b)[16] or could promote duplex formation though protein-RNA interactions[35]. To determine the effect of RNAP, we measured rates of duplex RNA formation by mixing asRNA with PC-containing scaffold alone or with reconstituted ePECs (containing ~20% free scaffold) and following the decrease in fluorescence signal (Fig. 1c; Online Methods). PC fluorescence decreased rapidly ($k_{obs,scaffold}$ = 1.5 ± 0.6 s^{-1}, $k_{obs,ensemble}$ = 0.94 ± 0.03 s^{-1} at 1 μM asRNA). To obtain the asRNA association rate, we determined k_{obs} as a function of asRNA concentration (Fig. 1d). After correcting for unbound scaffold, these measurements yielded an asRNA on-rate for the ePEC about half that observed for free scaffold ($k_{on,ePEC}$ = 0.31 ± 0.03 μM^{-1} s^{-1} *vs.* $k_{on,scaffold}$ = 0.76 ± 0.02 μM^{-1} s^{-1} Fig. 1f). These rates are comparable to previous estimates for formation of 8–20 bp duplexes (0.2–1.1 μM^{-1} s^{-1})[36–39]. To ensure that our measured rate of asRNA binding to ePECs reflected duplex formation in the RNAP exit channel and not binding to transiently dissociated scaffold followed by scaffold rebinding, we determined that the off-rate of scaffold from the ePEC was orders of magnitude slower in either the absence or presence of asRNA (Supplementary Fig. 2).

We next measured the dissociation rate (k_{off}) for asRNA release from the exit-channel RNA:RNA duplex or free scaffold duplex using a competitor RNA lacking PC. We first formed duplex-containing RNAs by annealing asRNA at 1 μM, and then mixed the duplex species with 250-fold excess competitor RNA (Fig. 1e). The time-dependent increase in PC fluorescence reflected regeneration of single-stranded PC-containing RNA as the asRNA transferred to the unlabeled competitor RNA (k_{off} = 0.10 ± 0.01 s^{-1}). RNAP had no effect on the asRNA off-rate, as the parallel experiment using PC scaffold alone gave a comparable dissociation rate constant (k_{off} = 0.10 ± 0.03 s^{-1}; Fig. 1f). Thus, the affinity of asRNA for scaffold *vs*. ePEC was stronger by a factor of ~2 (K_d of 130 ± 40 nM *vs.* 280 ± 90 nM, respectively). These off-rates and K_ds are consistent with those measured previously for DNA duplex dissociation[37] and cannot be explained by dissociation of the scaffold from the ePEC.

We conclude that the RNAP exit channel modestly inhibits asRNA binding to nascent RNA relative to an RNA not bound by RNAP (by a factor of ~2), and that the RNAP exit channel

principally affects the asRNA on-rate rather than off-rate. Thus, RNAP permits efficient structure formation despite the major steric constraint of the exit channel, but does not substantially stabilize nascent RNA structure (Fig. 1b). Effects of RNAP on duplex formation, rather than dissociation, are likely to be biologically relevant, since RNA structures, once formed, typically are stable on the time scale of transcription[5]. For these reasons and to simplify experiments, we focused subsequent measurements on asRNA association.

The RNAP flap tip slows duplex formation but aids pausing

We next asked how the RNAP flap tip affected formation and effects of nascent RNA structures. The flap domain forms one wall of the RNA exit channel near RNA nt −11 to −17, but makes little direct contact with the exiting RNA[35]. However, deletion of the flexible flap tip (β subunit residues 890–914 in *E. coli* RNAP; ΔFT1, Fig. 2a) prevents pause stimulation by the *his* pause hairpin even though the hairpin forms normally[20]. This result is disputed by Kuznedelov *et al.*[40], who report that a slightly larger deletion (884–914; ΔFT2, Fig. 2a) does not affect hairpin-stimulation of pausing and argue the 890–914 deletion interferes with pause hairpin formation. To clarify the effect of the flap tip on RNA structure formation and pausing, we purified both flap-tip deletion RNAPs and tested their effects on duplex-stimulation of pausing (Fig. 2b) and on duplex formation using asRNA. Neither flap-tip deletion affected the duration of the elemental pause, but both deletions eliminated duplex-stimulation of pausing either with or without NusA (Fig. 2c); NusA is known to enhance the effect of exit-channel duplexes with wild-type RNAP[23,24].

We next tested the effects of flap-tip deletions and of NusA on exit-channel duplex formation. Neither deletion reduced formation of the exit-channel duplex, as detected in the PC quenching assay (Fig. 2d). The smaller ΔFT1 deletion increased the rate of asRNA binding, close to that observed for scaffold RNA alone and consistent with removal of a steric block to duplex formation. The larger ΔFT2 deletion exhibited a rate of asRNA binding closer to wild-type RNAP, possibly because the bulky side chains or altered flap folding preserved steric interference with asRNA binding. NusA increased the asRNA binding to wild-type ePECs by a factor of ~2 (k_{obs} = 3.3 ± 0.2 s^{-1} *vs.* 1.8 ± 0.3 s^{-1} without NusA; Fig. 2d). Consistent with the sufficiency of NusA NTD for NusA stimulation of pausing[24], NusA NTD alone gave equivalent stimulation of asRNA binding. Both flap-tip deletions eliminated the ability of NusA to stimulate asRNA binding.

We conclude that the flap-tip is essential for the effect of exit-channel duplexes on pausing, but inhibits rather than promotes formation of the duplexes. These results conclusively establish that a duplex–flap tip interaction occurring after the duplex forms is necessary for pause stimulation by exit-channel RNA duplexes, consistent with previous proposals that steric clash between the duplex and the flap tip may promote duplex-induced clamp opening and consequent effects on the RNAP active site[20,22]. That NusA stimulates asRNA association to levels equivalent to those observed with free scaffold and that ΔFT1 gives similar asRNA association with or without NusA could suggest that NusA interaction relieves steric occlusion of asRNA binding by the flap tip.

Pause effect of exit-channel duplexes requires clamp opening

The RNA duplex–flap interaction required for hairpin-stimulation of pausing could be explained by consequences other than effects on clamp opening. For instance, flap–duplex interaction could inhibit translocation of nucleic acid through RNAP. Thus, we next sought to test directly for effects of exit-channel duplexes on clamp conformation and for effects of clamp conformation on the formation of exit-channel duplexes. For this purpose, we designed double cysteine variant RNAPs that were predicted to form disulfide bonds between the lid and flap domains in either the closed-clamp conformation (β′258iC-β1044C; based on *Tth*RNAP EC, pdb 2o5i)[35] or the open-clamp conformation (β′258iC-β843C; based on *Tth*RNAP ePEC, pdb 4gzy)[16] (Figs. 3a,b). β′258iC is an insertion of Cys between β′ 257G and β′ 258G in the lid domain; hereafter, the closed and open Cys-pairs are referred to as C and O.

We tested for formation of the expected crosslinks as a function of redox potential using non-reducing SDS-PAGE of reconstituted ePECs after incubation with mixtures of cystamine (CSSC) and DTT[21]. The C and O crosslinks were readily detected by the slower electrophoretic mobility of the crosslinked β′-β subunits (Figs. 3a,b). As the redox potential decreased, the fraction of crosslinked species increased as expected (Supplementary Fig. 3a,b). To study the effects of clamp conformation, we chose −0.22 V and −0.24 V for O and C, respectively, because they gave the highest fraction of crosslinking (~0.65 for both crosslinks).

We found that another oxidant, diamide, gave a higher fraction crosslinked for both C and O disulfide pairs (~0.9) than CSSC (Supplementary Fig. 4) but interfered with fluorescence measurements because it is chromophoric. Therefore, we performed kinetic assays with both oxidants to facilitate comparison to the asRNA binding assay.

We first tested whether stabilizing the clamp in the closed or open conformation with disulfide crosslinks affected duplex stimulation of pausing. We formed ePECs on the pause scaffold (Fig. 1a) and measured pause dwell times with and without exit-channel duplexes formed by addition of asRNA (Fig. 3c). CSSC had little effect on wild-type ePECs (Table 1)[21]. Further, uncrosslinked ePECs containing the C or O Cys pairs gave pause dwell times similar to wild-type ePECs with or without asRNA (Table 1), establishing that the Cys substitutions alone had little effect on pausing (a minor fraction of O ePEC, 0.1–0.2, remained crosslinked under reducing condition with a dwell time consistent with stabilized pausing). ePECs with a C crosslink but no exit-channel duplex also resembled wild-type, but C-crosslinked PECs containing an exit-channel duplex gave two pause fractions. One fraction (0.3, about equal to the ~0.35 uncrosslinked RNAP) had a long pause dwell time like wild-type or uncrosslinked PECs containing the exit-channel duplex (Fig. 3d **and** Supplementary Fig. 3c). The other fraction (0.7, about equal to the crosslinked RNAP) gave a much shorter dwell time (~10 s) equivalent to ePECs lacking an exit-channel duplex. We verified that the C crosslink eliminated the effect of an exit-channel duplex using diamide to increase the crosslink fraction to ~0.9 (Table 1; Supplementary Fig. 4c). Thus, stabilizing the clamp in the closed conformation with a disulfide prevented stimulation of pausing by an exit-channel duplex.

In contrast, the O-crosslinked ePEC appeared to be in a long-lived pause state resembling the duplex-stabilized PEC even when no duplex was present. Although asRNA increased the pause dwell time of the uncrosslinked O PEC similarly to wild type PEC (Table 1), after disulfide formation ~60% exhibited a long pause duration even without asRNA, consistent with the ~65% O crosslinked ePEC (Fig. 3e **and** Supplementary Fig. 3d). We confirmed this conclusion using diamide to generate ~90% O crosslinked ePECs (Table 1; Supplementary Fig. 4d). The crosslinked ePECs were not dissociated (Supplementary Fig. 5 f,g) and were active upon addition of NTPs to 0.5 mM (Supplementary Figs. 3c,d).

Taken together, our results suggest that most or all of the pause-stimulating effect of exit-channel duplexes can be explained by stabilization of the open-clamp conformation, with consequent effects on the RNAP active site. Inhibiting clamp opening with a disulfide crosslink eliminated most of the duplex-effect on pausing (from ≥10x to ≤3x; Table 1), whereas artificially stabilizing the open clamp using a disulfide stimulated pausing similarly to an exit-channel duplex but without the duplex.

Inhibiting clamp opening slows exit-channel duplex formation

Suppression of duplex effects by the C disulfide might be explained if the closed clamp prevents formation of exit-channel duplexes. To test whether clamp opening is required for or facilitates duplex formation, we tested asRNA binding to ePECs containing the C or O crosslink using the PC quenching assay (Figs. 3f,g). Uncrosslinked ePECs containing the C or O Cys pairs bound asRNA comparably to wild-type PECs (Supplementary Fig. 5b,e). However, asRNA binding to the C-crosslinked ePEC preparation (~20% unbound scaffold, ~50% C-crosslinked ePEC and ~30% uncrosslinked ePEC) exhibited three binding components that included slower asRNA binding to the crosslinked ePEC fraction (1.2 s^{-1} *vs*. 2.3 s^{-1} for uncrosslinked ePEC; Fig. 3f **and** Supplementary Fig. 5d,e). This result suggests that asRNA still binds the closed-clamp ePEC but stimulates pausing to a greatly reduced extent, in agreement with our previous observation of residual asRNA stimulation of pausing at high RfaH concentration[23]. In contrast, open-clamp crosslinked ePEC bound asRNA equivalently to uncrosslinked ePEC (Fig. 3g), suggesting the clamp opens readily in the absence of the crosslink.

Energetic coupling of active-site and exit-channel conformations

The finding that the open-clamp crosslink mimics duplex stimulation of pausing without a duplex strongly supports the view that the RNAP exit channel and active site are energetically linked through clamp position. To test the energetic linkage hypothesis in the opposite direction, we next examined the effects of pause-suppressing substitutions near the RNAP active site on asRNA binding in the exit channel. We hypothesized that if exit-channel-driven clamp opening can inhibit TL folding in the active site, then active-site alterations that suppress pausing should inhibit clamp opening and asRNA binding in the exit channel. To perform this test, we chose two previously identified substitutions known to inhibit pausing at the hairpin-stabilized *his* pause site[22,41,42]: β′F773V in the N-terminal portion of the bridge helix (BH) and βT563I in the conserved βDloopII, which interacts with both R780 in the BH and NTP in the RNAP active site (Fig. 4a). Although the mechanisms of pause suppression by these substitutions is not yet understood, they appear to involve F-

loop stabilization of TL folding through a network of contacts involving H777 and P750 (Fig. 4a)[21,22,27]. Consistent with earlier reports[22,43], F773V and T563I caused a substantial fraction of ePECs to bypass the duplex-stabilized state and react with NTP at rate similar to ePECs even after asRNA binding (60% or 84% of ePECs for T563I and F773V, respectively; Figs. 4b; T563I resembles the T563I, P560S double substitution studied earlier).

Consistent with clamp-mediated energetic linkage between the active site and the exit channel, the F773V and T563I substitutions also decreased the rate of asRNA binding to the nascent exiting RNA in ePECs (Figs. 4c,d). Although modest, these effects were reproducible and suggest that changes in the active site of RNAP, far from the exit-channel, can affect formation of exit-channel duplexes. Presumably, by favoring TL folding, the substitutions also favor the closed-clamp conformation. To confirm that inhibiting clamp opening inhibits duplex formation, we next tested whether the NusG paralog RfaH affects the rate of duplex formation. Consistent with previous results[23,25], RfaH inhibited duplex-stabilized pausing (Fig. 4b). As expected, ePECs bound by RfaH-NTD also exhibited a slower rate of exit-channel duplex formation (Figs. 4c,d). Together, our results support the idea that the exit channel and active site are energetically linked though clamp conformation and suggest that pause-suppressing alterations to RNAP outside the exit channel (F773V, T563I, and RfaH-NTD) inhibit asRNA binding to the nascent RNA by favoring a closed-clamp conformation of RNAP (Fig. 4e).

Exit-channel duplexes and NusA also inhibit translocation

Exit-channel duplexes appear to slow pause escape by two separate effects, inhibition of nucleic-acid translocation through RNAP and clamp comformation-mediated inhibition of TL folding required for catalysis[21,22,44]. To test directly for effects on translocation, we used a recently developed fluorescence assay in which unquenching of the guanosine analog 6-methylisoxanthopterin (6-MI) occurs upon translocation (Fig. 5a,b,c)[28]. We incorporated 6-MI in two versions of the ePEC scaffold, either in the nontemplate DNA (ntDNA) strand at +2 or in the template DNA (tDNA) strand at −8 (relative to the pause RNA 3′ nt at −1; Fig. 5a). To maximize the fluorescence signal[45,46], we adjusted the sequence context so that translocation of the 3′ U from the *i* to *i+1* site would melt an adjacent bp in which G was stacked on 6-MI, leaving 6-MI in a terminal bp stacked on a pyrimidine. These changes did not alter duplex-stabilization of pausing at U19, suggesting they should report duplex effects on translocation accurately.

We reacted C18 elongation complexes (ECs) formed on the 6-MI-containing ePEC scaffolds with UTP to form U19 ePEC in the pretranslocated register. Translocation would then unquench 6-MI fluorescence. Thus, the observed rate of fluorescence increase after UTP addition contains both U19 addition and translocation components (Fig. 5d,e,f)[28]. We measured the U19 addition rate separately (Table 2) and then calculated the translocation rate (Supplementary Fig. 6; Online Methods)[28]. Two effects of the exit-channel duplex were evident. First, the exit-channel duplex reduced the rate of translocation (Figs. 5g; Table 2). Second, the exit-channel duplex reduced the amplitude of the fluorescence increase to 35–50% of that observed without an exit-channel duplex (Figs. 5d,e,f). The simplest explanation

for the decrease in signal amplitude is that the majority of duplex-containing PEC remains in the pretranslocated register, which is consistent with prior studies[22]. Although a crystal structure of an ePEC formed on these same sequences using *Tth*RNAP is posttranslocated[16], multiple lines of biochemical evidence suggest that duplex-stablization returns the PEC to a mostly pretranslocated state with the RNA 3′ nt frayed off the DNA template[16,22]. We conclude that the exit-channel duplex both inhibits forward translocation of the PEC and shifts the equilibrium toward the pretranslocated register.

The RNAP flap-tip interacts with the *his* pause hairpin RNA and is required for duplex-enhancement of pausing (Fig. 2)[11,20]. Thus, we hypothesized that interaction of the flap tip and exit-channel duplex could explain the duplex inhibition of translocation. Consistent with the hypothesis, deletion of the flap tip abolished the exit channel-duplex effect on translocation (Fig. 5g). Combined with findings described above, this result indicates a dual function for flap-tip interaction with the exit-channel duplex: (1) it promotes clamp domain opening, with consequent effects on TL folding and catalysis in the RNAP active site, and (2) it inhibits translocation.

Effect of regulators on translocation at the *his* pause site

NusA and NusG have been proposed to affect translocation by RNAP. NusA reduces elongation rate, slows translocation, and prolongs pausing at sites stimulated by nascent RNA structures[24,47]. NusG and its paralog RfaH accelerate elongation, inhibit backtracking, and suppress duplex-stabilized pausing[23,48]. Using the 6-MI fluorescence assay, we measured translocation rates of ePECs with or without the exit-channel duplex, RfaH-NTD, or NusA. Consistent with previous results[47], NusA decreased the translocation rate, but only in the presence of the asRNA (Fig. 5h; Table 2). In contrast, RfaH increased translocation rate by decreasing duplex-inhibition of translocation (Fig. 5h; Table 2). These results confirm that NusA and RfaH affect translocation in ways that at least partially account for their synergy with exit-channel duplexes for effects on transcriptional pausing.

DISCUSSION

By implementing direct fluorescence detection of duplex formation in the nascent RNA, disulfide crosslinks that bias RNAP clamp position, and a fluorescence-based translocation assay[28], we gained new insights into regulatory connections between the RNA exit channel and RNAP catalytic center. First, we found that the RNAP exit channel allows structure formation with energetics similar to RNA outside the exit channel, with the same off-rate and an on-rate slower by only a factor of 2 (Fig. 1f) and adjustable by NusA (Fig. 2), RfaH (Fig. 4), and likely NusG[23]. Given that only 4–5 nt of the asRNA target is exposed to solution (Fig. 6b)[35] and that RNAP necessarily blocks more than half the routes of diffusive contact, the ability of asRNA to bind the target almost as fast as freely diffusible RNA (or as fast for ΔFT RNAP or in the presence of NusA) is remarkable and suggests the exit channel must have evolved to facilitate RNA structure formation. One possibility is that nascent RNA emerges from the mouth of the exit channel with its bases displayed for interaction.

Although intra-strand nascent RNA pairing may be faster than we measure for asRNA binding, competition for interaction with other nascent RNA segments may offset this local-

concentration effect[49]. At 5–10 μM, asRNA binding should occur on the timescale of nucleotide addition *in vivo* where pauses of ~1 s occur. Since these effective concentrations could easily be achieved by tethered RNA segments, our results suggest that modulation of exit-channel geometry by regulators could readily modulate RNA structure formation *in vivo*. Thus, RNAP not only determines the rate at which new segments become available for pairing, but also appears to modulate structure formation actively *via* changes in the properties of the RNA-exit channel. NusA-NTD and RfaH(NusG)-NTD augment this modulation by relieving steric inhibition though an interaction with the flap tip or increasing steric inhibition by stabilizing a closed clamp conformation, respectively (Figs. 2 **and** 4).

We found that clamp conformation also energetically links the RNA exit channel with the active site, consistent with previous results from Cys-pair reporters in the TL suggesting that exit-channel duplexes inhibit TL folding[21]. Trapping the clamp in the open conformation with a disulfide mimicked pause-enhancement by an exit-channel duplex even when no duplex was present (Fig. 3e). This result suggests the open clamp itself inhibits nucleotide addition in the active site. Importantly, the reverse linkage also occurs. Substitutions in the BH cap region over 35 Å from the clamp-BH/TL interface both suppress pausing, presumably by promoting TL folding (Fig. 4a,b), and decrease the rate of duplex formation in the exit channel (Fig. 4c,d), presumably by favoring a closed-clamp conformation (Fig. 6). Stabilizing the closed clamp with a disulfide both inhibited formation of an exit-channel duplex and eliminated most of the effect of the duplex on the active site. Together these results are readily explained if clamp opening alters BH/TL energetics *via* changes in the anchor (switches 1 and 2)[21,50] that disfavor TL folding, and if TL folding favors clamp closing, which inhibits formation of exit-channel duplexes[21,22]. Although we cannot exclude some other explanations (*e.g.*, clamp opening shifts RNA to a less favorable active-site orientation), the effects of cap substitutions on exit-channel duplex formation favor the model of energetic linkage between the BH/TL and exit channel *via* the clamp.

Strikingly, RNAP appears to have evolved so that significant changes in nucleotide addition rates are linked to relatively small energetic changes between conformational states. The closed-clamp conformation poses only a modest barrier to asRNA binding, especially without NusG or RfaH, but its opening strongly inhibits catalysis. The TL-folding mechanism appears poised to be sensitive to small changes such that regulatory interactions outside the TL can have large effects on pausing and nucleotide addition.

Our results also established that interaction of exit-channel duplexes with the flap tip slows translocation and likely explains why hairpin-stabilized pauses are preferentially pretranslocated with 3′-nucleotide fraying (Fig. 6).[22] Since the duplex forms even when clamp opening is inhibited (Fig. 5), the residual duplex inhibition seen in the closed-clamp crosslinked PEC (Table 1) likely reflects this effect on translocation. Consistent with prior kinetic, biochemical, and single-molecule studies of ECs[22,28,51], our results show that translocation and catalysis occur on similar time-scales in the PEC. Thus, NusA can increase pausing principally through effects on duplex-inhibited translocation (Fig. 5)[47], whereas RfaH can suppress pausing by promoting clamp closure and TL folding (Fig. 4)[21].

In conclusion, our results illustrate an active interplay between RNA structure formation in the RNAP exit channel and nucleotide addition in the active site of bacterial RNAP, mediated by clamp opening and modulated by elongation regulators. Recent findings establish that elemental pauses lacking RNA hairpin elements occur frequently *in vivo* and can exceed duplex-stabilized pauses in lifetime[15], but the role of clamp conformation in these pauses remains to be determined. Additionally, whether RNA structures and clamp movements similarly affect archaeal RNAP and eukaryotic RNAPII is unknown. The nascent structure formation assay and clamp-crosslinking approach described here should help address these questions.

ONLINE METHODS

Materials

DNA and RNA oligonucleotides (Supplementary Table 1) were obtained from IDT (Corvalville, IA); PC-containing oligonucleotides, from TriLink Biotechnologies (San Diego, CA); and 6-MI-containing oligonucleotides, from Fidelity Systems (Gaithersburg, MD). All oligonucleotides were purified by denaturing PAGE before use. [α-^{32}P]CTP was obtained from PerkinElmer Life Sciences; NTPs, from GE Healthcare (Piscataway, NJ); cystamine dihydrochloride (CSSC), from MP Biomedicals; DNA-modifying enzymes, from NEB or Agilent; and DNA purification reagents, from Promega. All other reagents were obtained from Sigma Aldrich or Fisher Scientific.

Plasmids and purification of RNAPs

Wild-type and variant RNAPs were overexpressed from plasmids (Supplementary Table 1). pRM795 is a T7 RNAP-based overexpression plasmid containing *E. coli rpoA*, *rpoZ*, *rpoB*, *rpoC*(PKA, His_{10}) that yields core RNAP ($\alpha_2\beta\beta'\omega$) with Protein Kinase A (PKA) and His_{10} tags on the C-terminus of β′. Plasmid pRM843 is a similar overexpression plasmid that instead yields core RNAP with a His_{10} tag on the N-terminus of β and Protein Kinase A (PKA) and Strep tags on the C-terminus of β′.

RNAPs were purified from *E. coli* BLR λDE3 transformed with the appropriate plasmids as previously described[21], with the following modifications to the purification protocol. For pRM843 derivatives, upon elution of samples from a heparin sepharose column, protein-containing fractions were pooled and dialyzed against 2 L buffer B (100 mM Tris HCl, pH 7.9, 150 mM NaCl, 0.1 mM EDTA, 5 mM β-mercaptoethanol) for 4 hr at 4 °C. Dialyzed RNAP was loaded onto a StrepTactin FPLC column (5 mL Strep-Tactin Superflow high capacity, IBA; GE Pharmacia AKTA Purifier, GE Biosciences), washed with 25 ml buffer B, and eluted with buffer B + 2.5 mM D-desthiobiotin. Fractions containing purified RNAPs were then dialyzed into RNAP storage buffer (20 mM Tris-HCl, pH 8.0, 250 mM NaCl, 20 μM $ZnCl_2$, 1 mM $MgCl_2$, 0.1 mM EDTA, 1 mM DTT, 50% glycerol) and stored at −80 °C in aliquots.

His-tagged full-length NusA and NusA-NTD were purified as described previously[24]. RfaH-NTD was purified from *E. coli* BL21 λDE3 cells harboring an overexpression plasmid, pIA777 (kindly provided by I. Artsimovitch), as described previously[23,55]. pIA777 encodes

an RfaH derivative with a TEV protease cleavage site between the NTD and CTD and a C-terminal His_6 tag.

Assembly of ePECs

Nucleic acid scaffolds used to reconstitute ePECs for *in vitro* transcriptional pause assays, stopped-flow asRNA binding measurements, and crosslinking assays were assembled as described previously[26]. Briefly, 10 μM RNA, 12 μM tDNA, and 15 μM ntDNA (Supplementary Table 1) were annealed in reconstitution buffer (RB; 10 mM Tris·HCl, pH 7.9, 40 mM KCl, 5 mM $MgCl_2$). Scaffolds were diluted with elongation buffer (EB; 25 mM HEPES-KOH, pH 8.0, 130 mM KCl, 5 mM $MgCl_2$, 1 mM dithiothreitol, 0.15 mM EDTA, 5% glycerol, and 25 μg of acetylated bovine serum albumin/mL) and incubated with RNAP for 15 min at 37 °C to form ePECs used for transcriptional pause assays and crosslinking assays. ePECs used for stopped-flow asRNA binding experiments were reconstituted in RB. For ePECs used in crosslinking assays, RNAP at 1 μM was the limiting component and was combined with 2 μM nucleic acid scaffold (1:2 RNAP: nucleic acid scaffold). For ePECs used in stopped-flow asRNA binding measurements, nucleic acid scaffold at 500 nM was limiting and was combined with 1.5 μM RNAP (3:1 RNAP: nucleic acid scaffold). Similarly, ePECs used for pause assays were reconstituted with excess of a scaffold at 150 nM and 100 nM RNAP (1:1.5 RNAP: nucleic acid scaffold with RNA as the limiting component).

To prepare ECs with fully complementary DNA strands and 6-MI for translocation measurements, C18 ECs were assembled using a modification of the reconstitution method described above. RNA (1 μM) and 0.5 μM tDNA (2:1 RNA: tDNA) were first annealed without ntDNA in RB buffer plus 5 mM $MgCl_2$ (10 mM Mg^{2+} final) followed by incubation with RNAP at 1.5 μM (3:1 RNAP:scaffold) in EB buffer at 37 °C for 15 min. ntDNA (2 μM) was then added and incubation was continued for an additional 15 min at 37 °C. For C18 ECs with 6-MI located in the tDNA strand (upstream FJ 6-MI scaffold; Fig. 5a), tDNA was limiting at 0.5 μM, and RNA and tDNA were at 1 μM and 2 μM, respectively (1:2:3:4 tDNA:RNA:RNAP:ntDNA). For C18 ECs with 6-MI located in the ntDNA strand (downstream FJ 6-MI scaffold; Fig. 5a), ntDNA was limiting at 0.5 μM and added to 0.75 μM C18 ECs lacking ntDNA formed by mixing RNA and tDNA at 1.5 μM and 0.75 μM, respectively, with 2.5 μM RNAP (1:3:1.5:5 ntDNA:RNA:tDNA:RNAP). In UMP incorporation measurements (quench-flow experiments; *e.g.*, Supplementary Fig. 6), RNA was limiting at 50 nM, tDNA at 100nM, RNAP at 150 nM, and ntDNA at 200 nM (1:2:3:4 RNA:tDNA:RNAP:ntDNA).

Cys-pair disulfide bond crosslinking assay

ePECs (1 μM) were reconstituted on a scaffold (6 μM T-5420; 8 μM NT-5069; 4 μM RNA-7418) with *E. coli* RNAP in EB buffer. Crosslinking of 1 μM ePECs was performed over a range of redox potentials (from −0.212 to −0.414 V) using 0.8 mM DTT plus CSSC (0.1, 0.2, 0.4, 0.6, 0.8, 1, 1.25, 1.5, 2, 2.5, 3 mM; *e.g.*, Supplementary Fig. 3) or diamide (0.1, 0.2, 0.4, 0.6, 0.8, 1.6, 3.2, 6.4, 12.8, 15, 20 mM final; *e.g.*, Supplementary Fig. 4) as the oxidant. These crosslinking experiments were performed at room temperature (RT) for 60 min. Samples were stopped by addition iodoacetamide to 15 mM. Formation of Cys-pair

crosslinks was evaluated by non-reducing SDS-PAGE (4–15% gradient Phastgel; GE) as described previously[21]. Gels were stained with Coomassie R and imaged with a CCD camera. The fraction crosslinked was quantified using ImageJ software. Experimental error was determined as the standard deviation in measurements from 3 independent replicates.

Transcriptional pausing assays

Pause assays in the presence or absence of 8-nt asRNA were performed as described previously[23]. ECs were reconstituted 2 nt upstream from the *his* pause site at 50 nM scaffold (T-5420; NT-5069; RNA-6593; yields G17 EC) with 200 nM core RNAPs and advanced to the U19 position by incubation with 2 μM [α-^{32}P]CTP and 100 μM UTP for 1 min at 37 °C in EB buffer. U19 ECs were then incubated with or without asRNA (1 μM final concentration) for 10 min at 37 °C. The pause assay was initiated by addition of GTP (10 μM final) to the U19 ePECs. Reaction samples were removed at 10, 20, 30, 40, 50, 60, 90, 120, 150, 180 s and quenched with an equal volume of 2× urea stop buffer (8 M urea, 50 mM EDTA, 90 mM Tris-borate buffer, pH 8.3, 0.02% bromphenol blue, and 0.02% xylene cyanol). After the final time point, all active ePECs were chased out of the paused state with high concentrations of GTP and UTP (500 μM each).

For reactions with NusA or RfaH-NTD, ECs were incubated with 2.5 μM full-length NusA, or 250 nM RfaH-NTD, which were added immediately after [α-^{32}P]CTP radiolabeling (*e.g.*, Fig. 2c **and** 4b). In experiments testing the effects of Cys-pair crosslinking on asRNA-mediated pausing, ECs were reconstituted as described above followed by oxidization of RNAPs in the ECs with 1 mM CSSC (closed Cys-pair RNAP) or 2 mM CSSC (open Cys-pair RNAP) and 0.8 mM DTT for 15 min at 37 °C. ECs were then radiolabeled and the pause assay time course was conducted as described above (*e.g.*, Fig. 3d,e). The reaction products were then separated on a denaturing 20% polyacrylamide gel in 0.5× TBE buffer[56]. Gels were exposed to phosphorimager screens, scanned using a Typhoon phosphorimager, and quantitated using the ImageQuant software (GE Healthcare). The RNA present in each lane was quantitated as a fraction of the total RNA in each lane and corrected for the unreacted fraction remaining in the chase lane (*e.g.*, Supplementary Fig. 3c,d). The rates of escape from the *his* pause site (*k*) was determined by single- or double-exponential fits of the fraction of U19/(>U19) as a function of time using KaleidaGraph (Synergy Software). Pause efficiencies or the fractions of paused elongation complexes (PEC) were estimated from the extrapolated intercept at time 0 as described previously[23,26].

Stopped-flow fluorescence assay of asRNA binding

ePECs (500 nM) assembled on a scaffold (1 μM T-5420; 1.5 μM NT-5069; 500 nM RNA-7604) containing pyrrolo-C (PC) RNA in RB was loaded in one syringe of the stopped-flow instrument (SF-300X, KinTek Corporation, Austin, TX, USA) and asRNA (RNA-6598) in RB was loaded in the other syringe. After rapid mixing at 37 °C, PC fluorescence was measured in real time using a 400-nm long-pass filter (Edmond Optics) and excitation at 337 nm (monochromator set to 4-nm bandwidth). The kinetics of PC fluorescence quenching were determined at various asRNA concentrations (*e.g.*, Fig. 1d) and averaged time traces from ≥3 replicates were fit to a single exponential equation (Eq. 1):

$$F_t = F_0 + A e^{-k_{obs} t} \quad (1)$$

where F_0 and F_t are the initial and final fluorescence intensity of PC, respectively; A is the amplitude of the fluorescent change; and k_{obs} is the pseudo-first-order observed rate constant of the decrease in PC fluorescence. To obtain a binding rate constant for the 8mer asRNA, k_{obs} was determined at various asRNA concentrations ranging from 0.5 to 64 μM. The resulting concentration dependence was fit to Eq. 2 and the bimolecular rate constant (on-rate; $k_{on,ensemble}$) was calculated from the slope of the line (see also Fig. 1d).

$$k_{obs} = k_{on,ensemble}[asRNA] + 0.1 \quad (2)$$

The y-intercept value (0.1), which is equal to k_{off}, was obtained from off-rate measurements (see below). To determine the rate of duplex formation on ePECs (the on-rate; $k_{on,\ ePEC}$) versus scaffold alone ($k_{on,\ scaffold}$), we fit the data to Eq. 3 and corrected for 20% unbound scaffold.

$$k_{on,ensemble} = (0.8 \times k_{on,ePEC}) + (0.2 \times k_{on,scaffold}) \quad (3)$$

For crosslinked samples, disulfide formation was initiated by incubating ePECs with 1 mM CSSC (closed-clamp crosslink) or 2 mM CSSC (open-clamp crosslink) and 0.8 mM DTT for 15 min at 37 °C prior to mixing with the 8mer asRNA in the stopped-flow instrument.

To determine the asRNA off-rate from the exit-channel RNA:RNA duplex in the PEC, ePECs were first reconstituted on a nucleic acid scaffold (1 μM T-5420; 1.5 μM NT-5069; 500 nM RNA-7604) in RB as described above. ePECs were then incubated with 2 μM asRNA (RNA-6598) for 10 min at 37 °C, resulting in the formation of the exit-channel duplex and the quenching of PC fluorescence. These quenched, duplex-containing PECs were challenged with 100 μM competitor RNA (RNA-7728) in the stopped-flow instrument and the increase in PC fluorescent signal was monitored as described above. The resulting fluorescent traces were fit to Eq. 4 to obtain the dissociation rate of asRNA from the duplex. To determine the rate of asRNA dissociation from the duplex in a scaffold without RNAP, the competition experiment was repeated in the absence of RNAP but otherwise using the same conditions.

$$F_t = F_0 + A(1 - e^{-k_{obs} t}) \quad (4)$$

where F_0 and F_t are the initial and final fluorescence intensity of PC, A_1 is the amplitude of the fluorescent change, and k_{obs} is the rate constant of PC fluorescence increase upon addition of the competitor RNA.

Stopped-flow fluorescence translocation assay

To measure translocation rates, we implemented an assay recently described by Belogurov and coworkers[28]. ECs (250 nM) were reconstituted at 250 nM scaffold lacking ntDNA (Fig. 5a; yields C18 EC) and 750 nM core RNAP in EB buffer at 37 °C 15 min followed by an additional incubation with 1 μM ntDNA for 20 min. Where indicated, 2 μM full-length NusA or 1.25 μM RfaH-NTD were incubated with C18 ECs for an additional 10 min prior to

incubating ECs with 2 μM CTP for 1 min at 37 °C in EB buffer. C18 ECs (20 μL) loaded in one syringe of the stopped-flow instrument were mixed rapidly with 200 μM UTP from the other syringe at 37 °C (both C18 ECs and UTP were in EB buffer + 5 mM $MgCl_2$, giving final concentrations of 10 mM Mg^{2+} and 200 μM UTP after mixing). 6-MI fluorophore was excited at 340 nm and the fluorescence of 6-MI emission was monitored in real time through a 400-nm long-pass filter (Edmund Optics). The resulting time traces were fit to a double-exponential equation (Eq. 5) to obtain the observed rate constant of the combination of the UTP addition and translocation.

$$F_t = F_0 + A_1\left(1 - e^{-k^1_{obs}t}\right) + A_2(1 - e^{-k^2_{obs}t}) \quad (5)$$

where F_0 and F_t are the initial and final fluorescence intensity of 6-MI; A_1 is the amplitude and k^1_{obs} is the rate constant for the major, fast phase of the reaction; and A_2 is the amplitude and k^2_{obs} is the rate constant for a minor slow phase (<20%) that corresponds to a minor fraction of C18 complex that adds UTP slowly. This minor, slow component was observed previously in similar pause assays[22] and by Belogurov and co-workers[28]. The rate of increase in 6-MI fluorescence after UTP addition is a composite of the rate of U19 addition followed by translocation, which generates the fluorescence increase (Fig. 5c). To calculate translocation rate, we directly measured U19 addition rate as described below (which also had the fast and slow rate components). Thus, to calculate the rate of translocation by newly formed U19 ePEC, we followed precedent[28] and used just the fast rate constants, k^1_{obs} and $k_{U19\text{-}fast}$ to obtain translocation rate (k_{trans}) from Eq. 6.

$$\frac{1}{k^1_{obs}} = \frac{1}{k_{trans}} + \frac{1}{k_{U19-fast}} \quad (6)$$

Rapid-quenched flow measurement of U19 addition

To obtain the rapid single-round UMP incorporation rate (Supplementary Fig. 6), C18 ECs (100 nM) were formed as described in the preceding section except that [α-^{32}P]CTP (2 μM) was used to form C18 ECs. For duplex-containing samples, ECs were then incubated with 4 μM asRNA. In a KinTek rapid quench-flow instrument, the preformed C18 ECs in syringe A were rapidly mixed with 400 μM UTP (prepared in EB supplemented with 5 mM $MgCl_2$) from syringe B to initiate UMP addition (10 mM Mg^{2+} and 200 μM UTP final after mixing). Samples were quenched with 2 M HCl, neutralized to pH 8.0 by addition of 3 M Tris, phenol-extracted, ethanol-precipitated, resuspended in 1× stop buffer, and then electrophoresed through denaturing 20% polycrylamide gels as described previously[21,26]. Gels were quantified using a Typhoon PhosphorImager and ImageQuant software (GE Healthcare). The relative fractions of C18/(>C18) RNAs as a function of time were quantified by fitting to a double exponential equation yielding $k_{U19\text{-}fast}$ and $k_{U19\text{-}slow}$ (Supplementary Figs. 6c, d). We used $k_{U19\text{-}fast}$ for translocation rate analyses because it represents the major fraction of ePEC (>75%).

Steady-state fluorescence measurement of asRNA binding

Steady-state fluorescence measurements of PC fluorescence intensity (Supplementary Fig. 1) were conducted on a PTI spectrofluorometer (Model QM-4/2003, Photon Technology International) using 10-mm path length and 50-μL quartz cuvettes (StarnaCells Inc, Atascadero, CA). Excitation spectra were obtained by recording fluorescence at 450 nm (8-nm bandwidth) while scanning excitation wavelengths between 300 and 400 nm (4-nm bandwidth). Emission spectra were obtained by monitoring fluorescence between 400 and 600 nm (8-nm bandwidth) and exciting at 337 nm (4-nm bandwidth) as described previously[30]. Experiments were conducted with five variations in RB buffer at 25 °C: (*i*) no oligonucleotide (RB solution); (*ii*) 1 μM ssRNA, which contains PC (RNA-7604); or (*iii*) dsRNA (to produce dsRNA, 1 μM of PC containing ssRNA, RNA-7604, was annealed to 2 μM of 8mer asRNA, RNA-6598, for 10 min at RT); (*iv*) 2 μM non-complementary RNA (1 μM of ssRNA was incubated with 2 μM non-complementary RNA, RNA-6753, for 10 min at RT); or (*v*) 1 μM non-fluorescent RNA (RNA-7418; Supplementary Table 1). Equilibrium binding and dissociation assays were performed by manually mixing 250 nM ssRNA (in 100 μL RB) with 1 μM 8mer asRNA oligo (RNA-6598) or with 1 μM noncomplementary 8mer RNA oligo (RNA-6753; as a control) in RB. After the fluorescence signal reached equilibrium, 8mer competitor RNA oligo (RNA-7728) was added to a final concentration of 2 μM.

Estimation of rates and kinetic modeling of asRNA binding

To calculate the observed rate of binding to the closed-clamp crosslinked ePEC, we fit fluorescent traces to a two-component model (model 1; 20% unbound scaffold, 80% ePECs) or a three-component model (model 2; 20% unbound scaffold, 50% C-crosslinked ePEC, and ~30% uncrosslinked ePEC) using KinTek Explorer Pro software, with off-rate constants fixed at 0.1 s^{-1} (Fig. 3f **and** Supplementary Fig. b,d).

Model 1:

$$\mathrm{ePEC}+\mathrm{asRNA}\underset{k_{-1}}{\overset{k_1}{\longleftrightarrow}}\mathrm{ePEC.asRNA}\ \ \mathrm{Scaffold}+\mathrm{asRNA}\underset{k_{-2}}{\overset{k_2}{\longleftrightarrow}}\mathrm{Scaffold.asRNA}$$

The on-rate of asRNA binding to ePEC was allowed to float while fixing the remaining rate constants to experimentally determined values (k_2 = 0.76 ± 0.02 μM^{-1} s^{-1}; k_{-1}, k_{-2} = 0.10 ± 0.01 s^{-1}).

Model 2:

$$\mathrm{ePEC}+\mathrm{asRNA}\underset{k_{-1}}{\overset{k_1}{\longleftrightarrow}}\mathrm{ePEC.asRNA}\ \ \mathrm{ePEC_{xlk}}+\mathrm{asRNA}\underset{k_{-2}}{\overset{k_2}{\longleftrightarrow}}\mathrm{ePEC_{xlk}.asRNA}\ \ \mathrm{Scaffold}+\mathrm{asRNA}\underset{k_{-3}}{\overset{k_3}{\longleftrightarrow}}\mathrm{Scaffold.asRNA}$$

The on-rate of asRNA binding to closed crosslinked ePEC ($ePEC_{xlk}$) was allowed to float while fixing the remaining rate constants (k_1 = 0.38 ± 0.02 μM^{-1} s^{-1}; k_2 = 0.76 ± 0.02 μM^{-1} s^{-1}; k_{-1}, k_{-2} = 0.10 ± 0.01 s^{-1}). The on-rate value (k_2 = 0.22 ± 0.02 μM^{-1} s^{-1}) obtained from

this fitting was used to determine the observed rate of asRNA binding to $ePEC_{xlk}$ using Eq. 2 (Fig. 3f).

Structural models of EC and PEC

The models representing the closed clamp EC and open clamp PEC shown in Figs. 1b, 2a, **and** 6 were generated using the program PyMOL version 1.6 (Schrödinger, LLC) and the PyMOL isosurface function to create low complexity surface representations. *E. coli* RNAP and nucleic acids in the EC were based on the pdb coordinates 2o5i and 3lu0[35,52]. The open-clamp conformation was modeled from pdb 4gzy[16]. The exit-channel RNA duplex was created as an A-form helix and oriented to avoid steric clash in the open-clamp PEC model.

Supplementary Material

Refer to Web version on PubMed Central for supplementary material.

Acknowledgements

We thank members of the Landick laboratory for many helpful discussions and for comments on the manuscript. This work was supported by US National Institutes of Health grants GM097458 to S.A.D. and GM038660 to R.L.

References

1. Nussinov R, Tinoco I Jr. Sequential folding of a messenger RNA molecule. J Mol Biol. 1981; 151:519–533. [PubMed: 6279861]
2. Brehm SL, Cech TR. Fate of an intervening sequence ribonucleic acid: excision and cyclization of the Tetrahymena ribosomal ribonucleic acid intervening sequence in vivo. Biochemistry. 1983; 22:2390–2397. [PubMed: 6860634]
3. Pan T, Sosnick T. RNA folding during transcription. Annu Rev Biophys Biomol Struct. 2006; 35:161–175. [PubMed: 16689632]
4. Matysiak M, Wrzesinski J, Ciesiolka J. Sequential folding of the genomic ribozyme of the hepatitis delta virus: structural analysis of RNA transcription intermediates. J Mol Biol. 1999; 291:283–294. [PubMed: 10438621]
5. Lai D, Proctor JR, Meyer IM. On the importance of cotranscriptional RNA structure formation. RNA. 2013; 19:1461–1473. [PubMed: 24131802]
6. Pan T, Artsimovitch I, Fang XW, Landick R, Sosnick TR. Folding of a large ribozyme during transcription and the effect of the elongation factor NusA. Proc Natl Acad Sci U S A. 1999; 96:9545–9550. [PubMed: 10449729]
7. Perdrizet GA 2nd, Artsimovitch I, Furman R, Sosnick TR, Pan T. Transcriptional pausing coordinates folding of the aptamer domain and the expression platform of a riboswitch. Proc Natl Acad Sci U S A. 2012; 109:3323–3328. [PubMed: 22331895]
8. Wong TN, Pan T. RNA folding during transcription: protocols and studies. Methods Enzymol. 2009; 468:167–193. [PubMed: 20946770]
9. Wickiser JK, Winkler WC, Breaker RR, Crothers DM. The speed of RNA transcription and metabolite binding kinetics operate an FMN riboswitch. Mol Cell. 2005; 18:49–60. [PubMed: 15808508]
10. Lewicki BT, Margus T, Remme J, Nierhaus KH. Coupling of rRNA transcription and ribosomal assembly in vivo. Formation of active ribosomal subunits in Escherichia coli requires transcription of rRNA genes by host RNA polymerase which cannot be replaced by bacteriophage T7 RNA polymerase. J Mol Biol. 1993; 231:581–593. [PubMed: 8515441]
11. Toulokhonov I, Artsimovitch I, Landick R. Allosteric control of RNA polymerase by a site that contacts nascent RNA hairpins. Science. 2001; 292:730–733. [PubMed: 11326100]

12. Nudler E. RNA polymerase backtracking in gene regulation and genome instability. Cell. 2012; 149:1438–1445. [PubMed: 22726433]
13. Zamft B, Bintu L, Ishibashi T, Bustamante C. Nascent RNA structure modulates the transcriptional dynamics of RNA polymerases. Proc Natl Acad Sci U S A. 2012; 109:8948–8953. [PubMed: 22615360]
14. Neuman KC, Abbondanzieri EA, Landick R, Gelles J, Block SM. Ubiquitous transcriptional pausing is independent of RNA polymerase backtracking. Cell. 2003; 115:437–447. [PubMed: 14622598]
15. Larson MH, et al. A pause sequence enriched at translation start sites drives transcription dynamics in vivo. Science. 2014; 344:1042–1047. [PubMed: 24789973]
16. Weixlbaumer A, Leon K, Landick R, Darst SA. Structural basis of transcriptional pausing in bacteria. Cell. 2013; 152:431–441. [PubMed: 23374340]
17. Herbert KM, et al. Sequence-resolved detection of pausing by single RNA polymerase molecules. Cell. 2006; 125:1083–1094. [PubMed: 16777599]
18. Landick R. The regulatory roles and mechanism of transcriptional pausing. Biochem Soc Trans. 2006; 34:1062–1066. [PubMed: 17073751]
19. Yakhnin AV, Babitzke P. Mechanism of NusG-stimulated pausing, hairpin-dependent pause site selection and intrinsic termination at overlapping pause and termination sites in the Bacillus subtilis trp leader. Mol Microbiol. 2010; 76:690–705. [PubMed: 20384694]
20. Toulokhonov I, Landick R. The flap domain is required for pause RNA hairpin inhibition of catalysis by RNA polymerase and can modulate intrinsic termination. Mol Cell. 2003; 12:1125–1136. [PubMed: 14636572]
21. Nayak D, Voss M, Windgassen T, Mooney RA, Landick R. Cys-pair reporters detect a constrained trigger loop in a paused RNA polymerase. Mol Cell. 2013; 50:882–893. [PubMed: 23769674]
22. Toulokhonov I, Zhang J, Palangat M, Landick R. A central role of the RNA polymerase trigger loop in active-site rearrangement during transcriptional pausing. Mol Cell. 2007; 27:406–419. [PubMed: 17679091]
23. Kolb KE, Hein PP, Landick R. Antisense oligonucleotide-stimulated transcriptional pausing reveals RNA exit channel specificity of RNA polymerase and mechanistic contributions of NusA and RfaH. J Biol Chem. 2014; 289:1151–1163. [PubMed: 24275665]
24. Ha KS, Toulokhonov I, Vassylyev DG, Landick R. The NusA N-terminal domain is necessary and sufficient for enhancement of transcriptional pausing via interaction with the RNA exit channel of RNA polymerase. J Mol Biol. 2010; 401:708–725. [PubMed: 20600118]
25. Sevostyanova A, Belogurov GA, Mooney RA, Landick R, Artsimovitch I. The beta subunit gate loop is required for RNA polymerase modification by RfaH and NusG. Mol Cell. 2011; 43:253–262. [PubMed: 21777814]
26. Kyzer S, Ha KS, Landick R, Palangat M. Direct versus limited-step reconstitution reveals key features of an RNA hairpin-stabilized paused transcription complex. J Biol Chem. 2007; 282:19020–19028. [PubMed: 17502377]
27. Malinen AM, et al. CBR antimicrobials alter coupling between the bridge helix and the beta subunit in RNA polymerase. Nat Commun. 2014; 5:3408. [PubMed: 24598909]
28. Malinen AM, et al. Active site opening and closure control translocation of multisubunit RNA polymerase. Nucleic Acids Res. 2012; 40:7442–7451. [PubMed: 22570421]
29. Berry DA, Jung KY, Wise DS, Sercel AD, Pearson WH, Mackie H, Randolph JB, Somers RL. Pyrrolo-dC and pyrrolo-C: Fluorescent analogs of cytidine and 2′-deoxycytidine for the study of oligonucleotides. Tetrahedron Lett. 2004; 45:2457–2461.
30. Tinsley RA, Walter NG. Pyrrolo-C as a fluorescent probe for monitoring RNA secondary structure formation. RNA. 2006; 12:522–529. [PubMed: 16431979]
31. Liu C, Martin CT. Fluorescence characterization of the transcription bubble in elongation complexes of T7 RNA polymerase. J Mol Biol. 2001; 308:465–475. [PubMed: 11327781]
32. Liu C, Martin CT. Promoter clearance by T7 RNA polymerase. Initial bubble collapse and transcript dissociation monitored by base analog fluorescence. J Biol Chem. 2002; 277:2725–2731. [PubMed: 11694519]

33. Johnson NP, Baase WA, von Hippel PH. Investigating local conformations of double-stranded DNA by low-energy circular dichroism of pyrrolo-cytosine. Proc Natl Acad Sci U S A. 2005; 102:7169–7173. [PubMed: 15883388]
34. Dash C, Rausch JW, Le Grice SF. Using pyrrolo-deoxycytosine to probe RNA/DNA hybrids containing the human immunodeficiency virus type-1 3' polypurine tract. Nucleic Acids Res. 2004; 32:1539–1547. [PubMed: 15004241]
35. Vassylyev DG, Vassylyeva MN, Perederina A, Tahirov TH, Artsimovitch I. Structural basis for transcription elongation by bacterial RNA polymerase. Nature. 2007; 448:157–162. [PubMed: 17581590]
36. Braunlin WH, Bloomfield VA. 1H NMR study of the base-pairing reactions of d(GGAATTCC): salt effects on the equilibria and kinetics of strand association. Biochemistry. 1991; 30:754–758. [PubMed: 1988062]
37. Cisse II, Kim H, Ha T. A rule of seven in Watson-Crick base-pairing of mismatched sequences. Nat Struct Mol Biol. 2012; 19:623–627. [PubMed: 22580558]
38. Kinjo M, Rigler R. Ultrasensitive hybridization analysis using fluorescence correlation spectroscopy. Nucleic Acids Res. 1995; 23:1795–1799. [PubMed: 7784185]
39. Wetmur JG. DNA probes: applications of the principles of nucleic acid hybridization. Crit Rev Biochem Mol Biol. 1991; 26:227–259. [PubMed: 1718662]
40. Kuznedelov KD, Komissarova NV, Severinov KV. The role of the bacterial RNA polymerase beta subunit flexible flap domain in transcription termination. Dokl Biochem Biophys. 2006; 410:263–266. [PubMed: 17286098]
41. Artsimovitch I, Chu C, Lynch AS, Landick R. A new class of bacterial RNA polymerase inhibitor affects nucleotide addition. Science. 2003; 302:650–654. [PubMed: 14576436]
42. Landick R, Stewart J, Lee DN. Amino acid changes in conserved regions of the beta-subunit of Escherichia coli RNA polymerase alter transcription pausing and termination. Genes Dev. 1990; 4:1623–1636. [PubMed: 2253882]
43. Svetlov V, Belogurov GA, Shabrova E, Vassylyev DG, Artsimovitch I. Allosteric control of the RNA polymerase by the elongation factor RfaH. Nucleic Acids Res. 2007; 35:5694–5705. [PubMed: 17711918]
44. Zhang J, Palangat M, Landick R. Role of the RNA polymerase trigger loop in catalysis and pausing. Nat Struct Mol Biol. 2010; 17:99–104. [PubMed: 19966797]
45. Hawkins ME. Fluorescent pteridine probes for nucleic acid analysis. Methods Enzymol. 2008; 450:201–231. [PubMed: 19152862]
46. Rist MJ, Marino JP. Fluorescent nucleotide base analogs as probes of nucleic acid structure, dynamics and interactions. Current Organic Chemistry. 2002; 6:775–793.
47. Zhou J, Ha KS, La Porta A, Landick R, Block SM. Applied force provides insight into transcriptional pausing and its modulation by transcription factor NusA. Mol Cell. 2011; 44:635–646. [PubMed: 22099310]
48. Herbert KM, et al. E. coli NusG inhibits backtracking and accelerates pause-free transcription by promoting forward translocation of RNA polymerase. J Mol Biol. 2010; 399:17–30. [PubMed: 20381500]
49. Lubkowska L, Maharjan AS, Komissarova N. RNA folding in transcription elongation complex: implication for transcription termination. J Biol Chem. 2011; 286:31576–31585. [PubMed: 21730066]
50. Cramer P, Bushnell D, Kornberg R. Structural basis of transcription: RNA polymerase II at 2.8 Å resolution. Science. 2001; 292:1863–1876. [PubMed: 11313498]
51. Dangkulwanich M, et al. Complete dissection of transcription elongation reveals slow translocation of RNA polymerase II in a linear ratchet mechanism. Elife. 2013; 2:e00971. [PubMed: 24066225]
52. Opalka N, et al. Complete structural model of Escherichia coli RNA polymerase from a hybrid approach. PLoS Biol. 2010; 8
53. Artsimovitch I, Svetlov V, Murakami K, Landick R. Co-overexpression of *E. coli* RNA polymerase subunits allows isolation and analysis of mutant enzymes lacking lineage-specific sequence insertions. J. Biol. Chem. 2003; 278:12344–12355. [PubMed: 12511572]

54. Vassylyev DG, et al. Structural basis for substrate loading in bacterial RNA polymerase. Nature. 2007; 448:163–168. [PubMed: 17581591]

55. Belogurov GA, et al. Structural basis for converting a general transcription factor into an operon-specific virulence regulator. Mol Cell. 2007; 26:117–129. [PubMed: 17434131]

56. Hein PP, Palangat M, Landick R. RNA transcript 3'-proximal sequence affects translocation bias of RNA polymerase. Biochemistry. 2011; 50:7002–7014. [PubMed: 21739957]

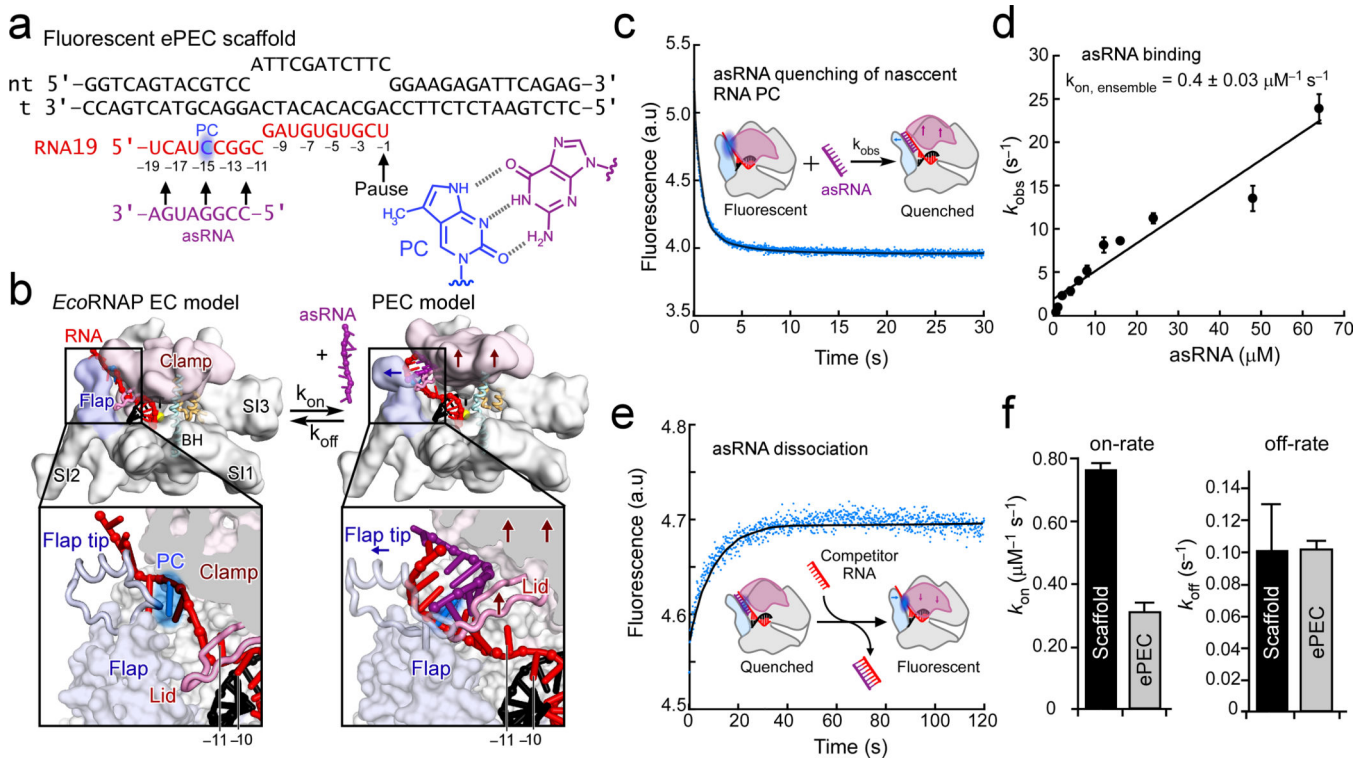

Figure 1. Modest inhibition of RNA:RNA duplex formation by RNAP

(**a**) The ePEC nucleic-acid scaffold (Table S1). DNA strands are shown in black, RNA in red, Pyrrolo-C (PC) in blue, and the 8-mer asRNA oligo in purple. The position of the pause (U19; −1 from 3′ end) is indicated by an arrow.

(**b**) Models of *E. coli* RNAP EC and PEC. Left, closed-clamp, active EC model (based on PDB 2o5i and 3lu0[35,52]) showing clamp (light pink), flap (light blue), bridge helix (BH; cyan), and location of major *E.coli* sequence insertions (SI1, SI2, SI3)[52,53]. The RNA:DNA hybrid (red and black), the exiting RNA (red), and asRNA (purple) are indicated. Right, model of open-clamp, duplex-stabilized PEC containing *E. coli* RNAP (based on PDB 4gzy[16]) with arrows indicating clamp and flap movement upon duplex formation. The blow-up shows the location of the lid (pink), flap-tip, and PC (blue), which is quenched by duplex formation with asRNA in the PEC.

(**c**) An averaged time trace of PC fluorescence (n = 6) after mixing 1 μM asRNA with 250 nM ePECs.

(**d**) asRNA concentration dependence of PC-quenching for ePECs. The slope of the linear regression line yields the average on-rate ($k_{on,ensemble}$) of asRNA binding to ePECs (~80%) and free scaffold (~20%).

(**e**) asRNA dissociation as monitored by PC fluorescence increase after addition of 100 μM competitor RNA to 500 nM preformed duplex-stabilized PEC (averaged trace; n=3).

(**f**) The bimolecular rate constants of RNA duplex formation and asRNA dissociation in ePECs or free scaffold. Error bars, s.d. (n = 3).

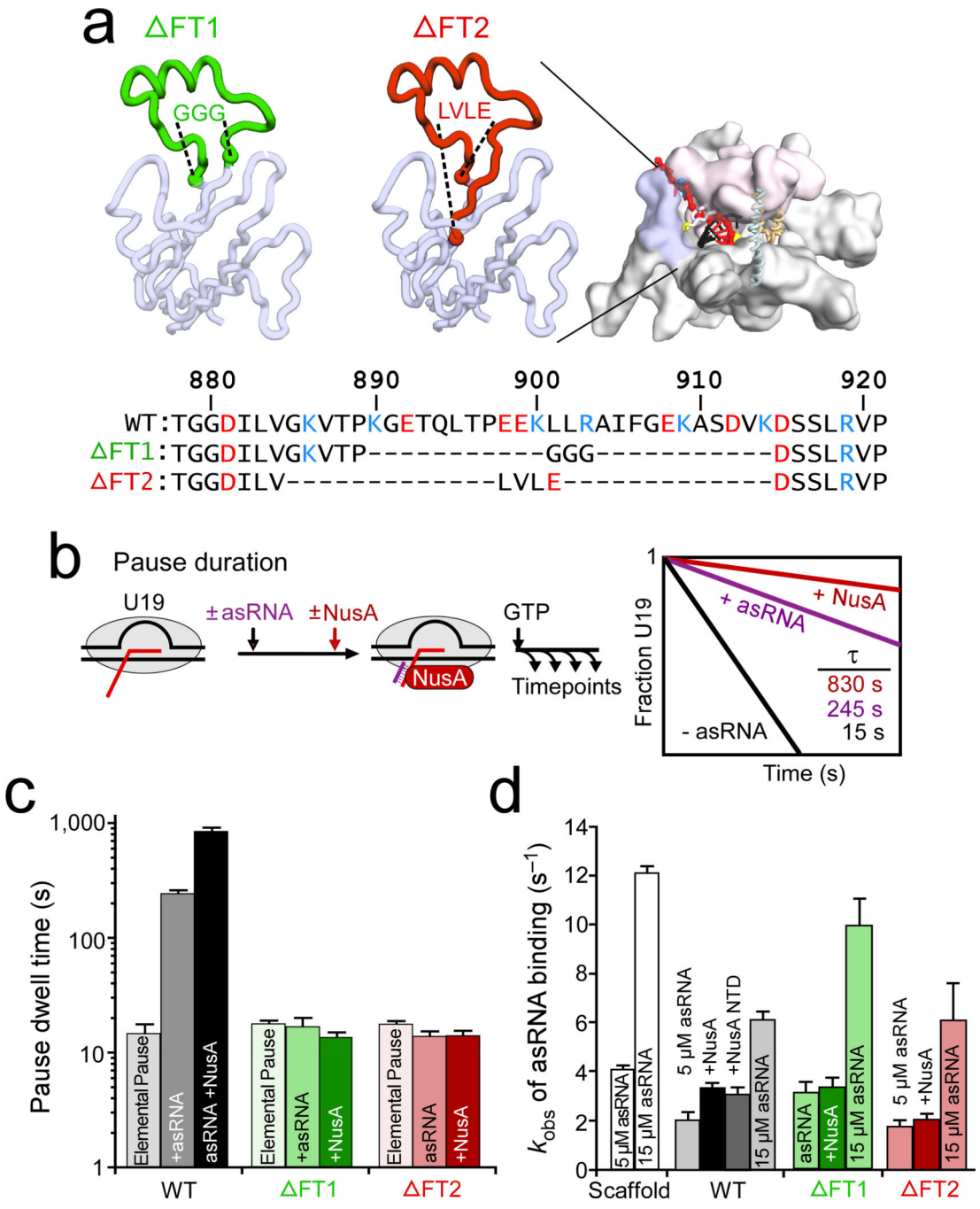

Figure 2. Effects of the flap-tip deletion on duplex-stabilized pausing and exit-channel duplex formation

(**a**) Structural model of an *E.coli* RNAP EC showing the β flap region (light blue) and the location of two β flap-tip deletions highlighted in green (ΔFT1) or red (ΔFT2). The β flap-tip sequences of wild-type and the two flap-tip deletions are shown (red, acidic amino acids; blue, basic amino acids).

(**b**) Schematic of pause duration experiment. ECs were reconstituted on an ePEC scaffold 2-nt before the pause site (G17 EC) and incubated with 2 μM [α-^{32}P]CTP to extend to C18.

UTP and GTP were then added to elongate through the *his* pause site (U19); pause half-lives of ePECs were measured (Online Methods). The plot shown depicts the effect of asRNA and NusA[23] for wild-type RNAP.

(**c**) Effect of flap-tip deletions on asRNA-stabilized pausing with or without asRNA or full-length NusA (2.5 μM). Error bars, s.d. (n = 3).

(**d**) The observed rate of the duplex formation (k_{obs}) for the scaffold alone (Fig. 1a) or for ePECs containing wild-type and ΔFT RNAPs. k_{obs} values were determined with 5 μM or 15 μM asRNA in the absence or presence of full-length NusA (2.5 μM) or 4 μM NusA-NTD at 37 °C. Error bars, s.d. (n = 3).

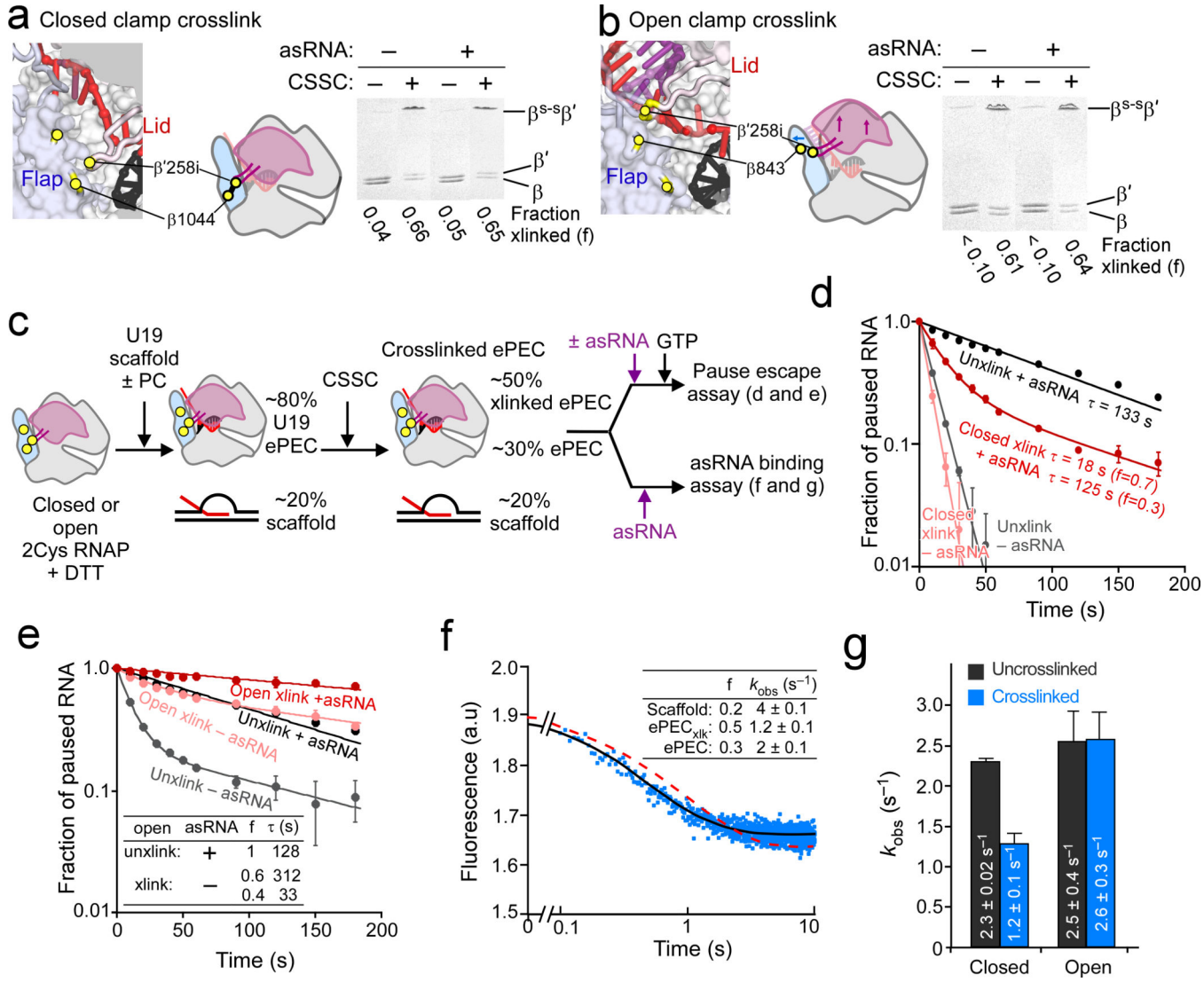

Figure 3. Effects of closed- and open-clamp crosslinks on duplex formation and duplex-stabilized pausing

(**a,b**) Position and detection of closed (**a**) and open (**b**) Cys-pair crosslinks. Blow-ups depict all three Cys locations: an insertion after β′G258 and substitutions for βP1044 or βT843. The crosslinked (xlinked) fractions are shown below a non-reducing SDS-PAGE gel. Uncropped gels are shown in Supplementary Fig. 3.

(**c**) Experimental scheme to test effects of closed- and open-clamp crosslinks on pausing and on asRNA binding.

(**d**) Pausing by the closed-clamp Cys pair after CSSC treatment (xlink) or in reducing conditions (unxlink) with and without an exit-channel duplex. The fraction of remaining U19 RNA was plotted as a function of reaction time.

(**e**) Pausing by the open-clamp Cys pair after CSSC treatment (xlink) or in reducing conditions (unxlink) with and without an exit-channel duplex. Inset table shows the fraction crosslinked (f) and dwell times (τ) of the uncrosslinked (unxlink) sample with asRNA and the crosslinked sample without asRNA.

(**f**) Averaged dataset (n = 5) showing the decrease in fluorescence of pyrrolo-C upon duplex formation in closed-clamp, crosslinked (xlk) ePECs. Data were fit to both a model containing a single population of ePECs combined with ~20% free scaffold (red line) and a containing two populations of ePECs (black line). Inset, fractions and rates for each component and of fluorescence quenching.

(**g**) Measured rates of 5 μM asRNA association with closed- and open-clamp Cys-pair ePECs with and without crosslinking after correction for unbound scaffold. Error bars, s.d. (n = 3).

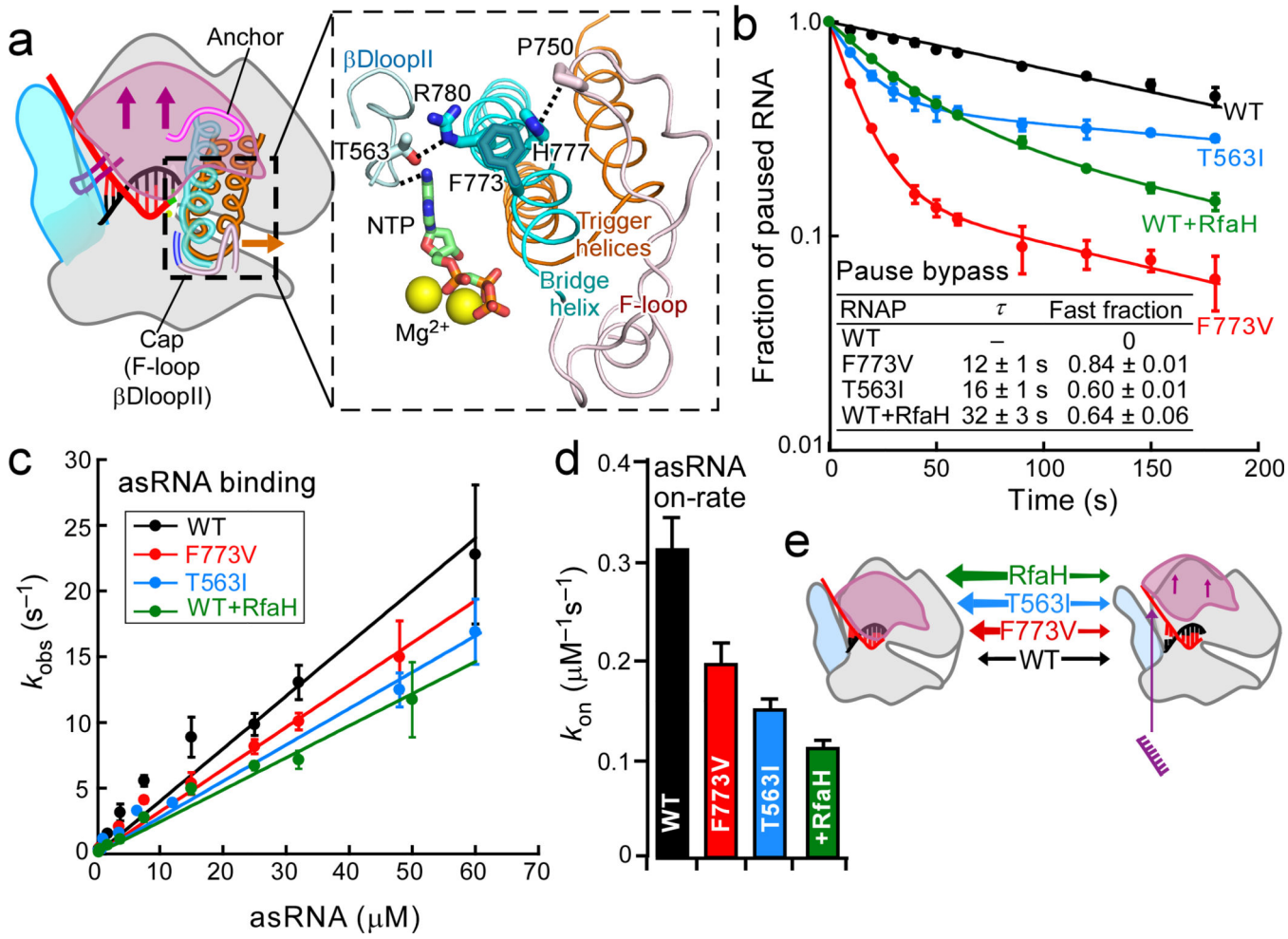

Figure 4. Effects of pause-suppressing substitutions and RfaH on duplex formation and duplex-stabilized pausing

(**a**) Schematic of the *E. coli* EC with inset showing the cap region based on *Tth*EC bound to NTP (pdb 2o5j)[54], the bridge helix (cyan), trigger helices (orange), βDloopII (light blue), F-loop (light pink), and active-site Mg^{2+} (yellow). Side chains are shown for T563 and F773, positions of pause suppressing substitutions, and for R780, H777, and P750, which form a network of interactions that may stabilize a paused conformation of the TL, or when disrupted, may aid TL folding *via* F loop positioning[22,27,41].

(**b**) Fraction of U19 RNA in duplex-stabilized PECs as a function of time. The pause dwell times (τ) were determined as shown in Fig. 2b by fitting the disappearance of U19 RNA to a single exponential (for wild-type) or to a double exponential (for mutant RNAPs and wild-type RNAP + RfaH-NTD). Error bars, s.d. (*n* = 3). Inset, fractions of PECs that bypass the duplex-stabilized pause state.

(**c**) The asRNA-concentration dependence of the observed rate of PC fluorescence quenching (k_{obs}) for wild-type, F773V, T563I, and wild-type plus 2.5 μM RfaH-NTD.

(**d**) The calculated on-rates (k_{on}) of the asRNA binding to the nascent RNA in ePECs containing wild-type, F773V, or T563I RNAPs, and wild-type RNAP in the presence of 2.5 μM RfaH-NTD. Error bars, s.d. (*n* = 3).

(**e**) Schematic of the effects of pause-suppressing substitutions and RfaH-NTD on clamp opening. Arrows sizes represent shifts in the equilibrium between closed- and open-clamp conformations.

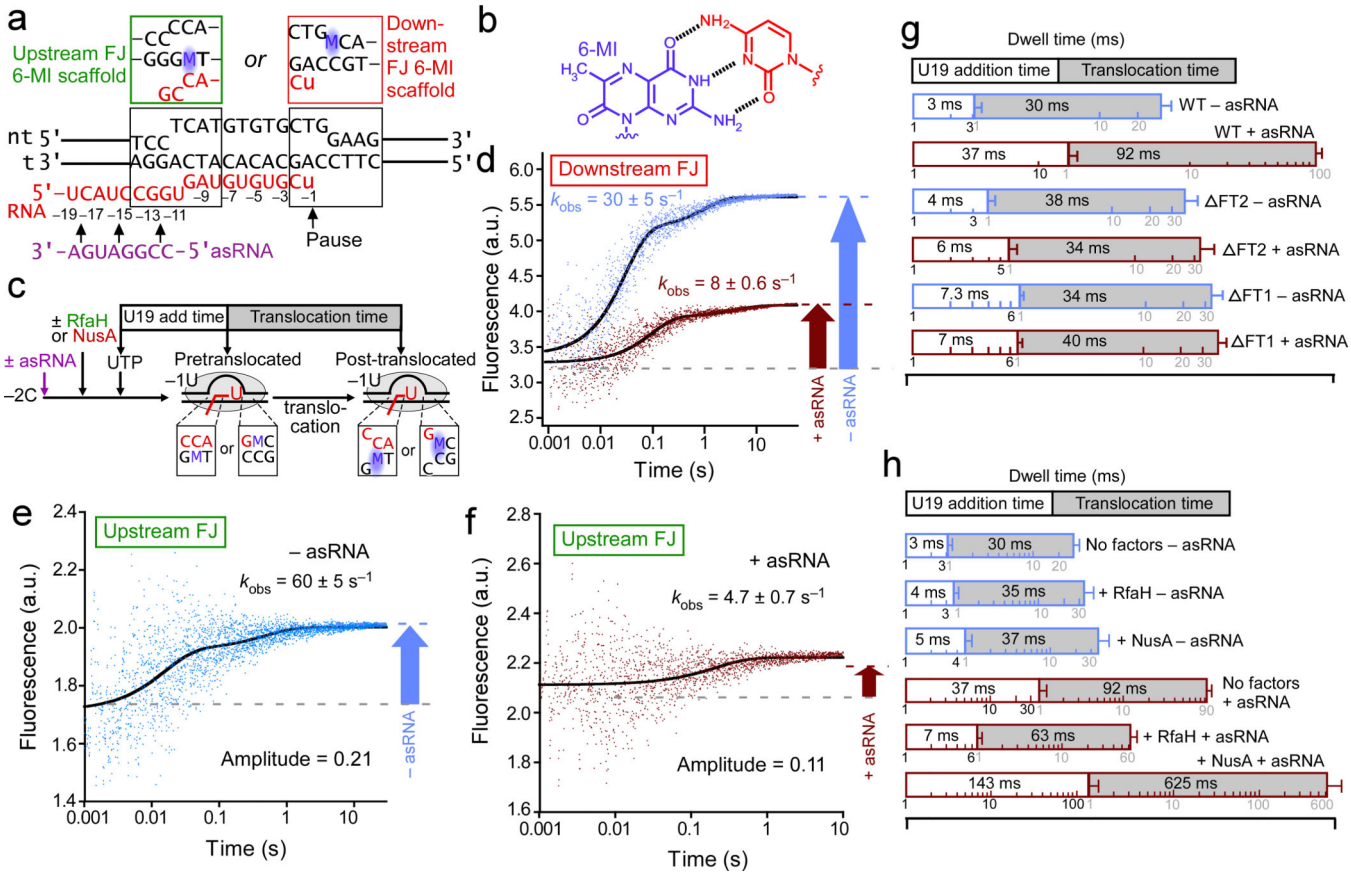

Figure 5. asRNA, flap-tip, NusA, and RfaH-NTD effects on forward translocation

(**a**) Upstream fork junction (FJ; green box) and downstream FJ (red box) scaffolds modified from the original (black box) ePEC scaffold and used for 6-MI translocation assays[28].

(**b**) 6-MI base pair with cytosine.

(**c**) Schematic of reactions used to measure translocation rates. Changes that occur in FJs of the transcription bubble upon translocation and resultant effects on 6-MI fluorescence are depicted.

(**d**) Time-resolved measurements of the increase in downstream-FJ 6-MI fluorescence upon UMP incorporation and subsequent translocation for ePECs with or without 4 μM asRNA. Fluorescence intensity is shown in arbitrary units (a. u.). The amplitudes of fluorescence changes in the presence or absence of asRNA are indicated by solid arrows.

(**e,f**) Time-resolved measurements of the increase in upstream-FJ 6-MI fluorescence upon UMP incorporation and subsequent translocation for ePECs with (**e**) or without (**f**) 4 μM asRNA. The amplitudes of fluorescence changes in the presence or absence of asRNA are indicated by solid arrows.

(**g**) Dwell times of UMP addition and translocation for wild-type and ΔFT RNAPs in the presence or absence of asRNA.

(**h**) Effects of NusA and RfaH-NTD on UMP addition and translocation. Error bars in **g–h**, s.d. (n = 3).

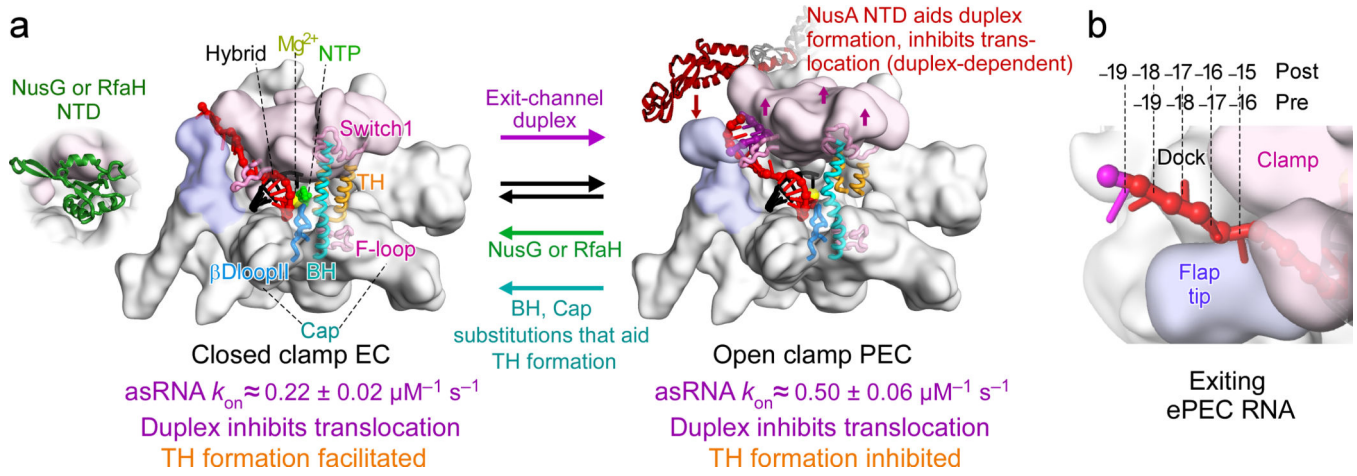

Figure 6. Effects of clamp position, regulators, and cap-region substitutions on exit-channel duplex formation and on pausing

(**a**) Closed- and open-clamp conformations of the transcription complex indicating the calculated rates of asRNA binding to the nascent RNA, effects of clamp conformation on TL folding into the trigger helices (TH), and effects of the exit-channel duplex on translocation. The asRNA on-rates were calculated from results in Fig. 4 assuming an off-rate of 0.1 ± 0.01 s^{-1}. The ~4× effect of the duplex on translocation in both closed and open states is inferred from the measured effect in wild-type PECs and the retention of a 3–4× duplex effect on pause escape when the clamp is crosslinked closed or open (Table 1). The effects of the exit-channel duplex, regulators, and cap substitutions on the equilibrium between closed and open conformations are indicated by arrows.

(**b**) Exiting RNA available for asRNA binding in the ePEC model containing a 19-nt RNA. The red nucleotide positions will be exposed in the pretranslocated register (4 nucleotides exposed, −16 to −19). The magenta nucleotide position will additionally be exposed in the posttranslocated register (5 nucleotides exposed, −15 to −19).

Table 1

Pause dwell times (τ) of PECs formed by wild-type, C, or O RNAPs treated with CSSC or diamide.

		Wild-type RNAP		Closed Cys-pair RNAP			Open Cys-pair RNAP		
Oxidant	**Exit channel duplex**	**τ (s)**	**Kinetic fraction**	**xlink Fraction**	**τ (s)**	**Kinetic fraction**	**xlink Fraction**	**τ (s)**	**Kinetic fraction**
none	−	10 ± 0.4	1	0.04 ± 0.007	10 ± 0.1	1	0.15 ± 0.06	11 ± 0.4 160 ± 16	0.77 ± 0.1 0.23 ± 0.1
	+	133 ± 7	1	0.05 ± 0.02	108 ± 6	1	0.14 ± 0.07	128 ± 6	1
CSSC[a]	−	11 ± 0.1	1	0.64 ± 0.03	6.6 ± 0.3	1	0.60 ± 0.04	312 ± 97 33 ± 10	0.60 ± 0.1 0.40 ± 0.1
	+	160 ± 8	1	0.61 ± 0.04	18 ± 1 125 ± 15	0.72 ± 0.04 0.28 ± 0.04	0.60 ± 0.05	450 ± 32	1
Diamide[b]	−	29 ± 1[b]	0.45 ± 0.01[b]	0.86	19 ± 1	0.45 ± 0.01	0.85	322 ± 24	0.7 ± 0.01
	+	270 ± 7[b]	0.68 ± 0.01[b]	0.90	26 ± 1	0.44 ± 0.1	0.86	1500 ± 220	0.72 ± 0.01

The pause dwell-time was calculated from the rate of pause escape on the scaffold, which can form the 8-bp RNA:RNA duplex when the as RNA oligo is present, using an *in vitro* transcription pause assay as described in Online Methods.

[a] ePECs halted at the pause site (U19) were treated with 1mM CSSC (closed-clamp crosslink) or 2 mM CSSC (open-clamp crosslink) and 0.8 mM DTT (E_h = −0.24 V for closed-clamp crosslink or −0.22 V for open-clamp crosslink) with fraction crosslinked of ePECs containing C and O RNAPs being ~0.7 and 0.61, respectively (Fig. 3a,d). The fraction of complexes attributable to each species was obtained by fitting U19 pause RNA concentration as a function of time to a two-exponential decay equation.

[b] In these experiments, ECs halted at 2nt before the pause (C18) were treated with 15 mM diamide and 0.8 mM DTT and elongated through the pause site (U19) on the *his* pause scaffold (Fig. 1a). Fraction represents the pause efficiency (fraction of RNAPs that recognize the pause).

Table 2

Effect of exit-channel duplex formed with 8mer asRNA on the rate of translocation by ePECs containing WT RNAP, WT RNAP and regulators, and mutant RNAPs

		Overall Rate[a] (s^{-1})	UTP addition rate[b] (s^{-1})	Translocation Rate (s^{-1})
WT RNAP	−	30 ± 5	350 ± 50	33 ± 6
	+ duplex	8 ± 0.6	30 ± 6	11 ± 2
ΔFT1 RNAP	−	24 ± 5	137 ± 6	29 ± 6
	+ duplex	21 ± 3	148 ± 6	25 ± 4
ΔFT2 RNAP	−	24 ± 5	249 ± 27	27 ± 7
	+ duplex	25 ± 4	165 ± 27	29 ± 9
WT RNAP + RfaH	−	27 ± 9	275 ± 34	30 ± 11
	+ duplex	14 ± 1.5	146 ± 21	16 ± 3
WT RNAP + NusA	−	24 ± 7	198 ± 34	27 ± 10
	+ duplex	1.3 ± 0.3	7 ± 1.5	1.6 ± 0.7

[a] Overall rate represents the composite rate of translocation and UTP addition calculated from the fluorescence increase of 6-MI incorporated at the +2 position in the ntDNA upon addition of UTP (Fig. 5a).

[b] The UTP addition rate ($k_{U19\text{-}fast}$) of different complexes were obtained from the rate of appearance of U19 RNA on the same scaffold used to determine overall rate using rapid-quench flow method as described in Online Methods (Supplementary Fig. 6). Errors are standard deviations from experimental triplicates or are propagated error (translocation rate).